Mechanics of Advanced Composite Structures

Journal homepage: https://macs.semnan.ac.ir/

Semnan University

ISSN: 2423-7043

Research Article

Meshfree Approach for the Torsional Analysis of Orthotropic and FGM Thin-Walled Open Sections

Ram Bilas Prasad[a*], Rahul Kumar[b], Jeeoot Singh[c]

[1,3]Madan Mohan Malaviya University of Technology, Gorakhpur, U.P, 273010, India
[2]Department of Mechanical Engineering, DDU Gorakhpur University
Corresponding author email id: rbpme@mmmut.ac.in

ARTICLE INFO

Article history:

Received: 2023-10-19
Revised: 2024-03-22
Accepted: 2024-05-12

Keywords:

Torsion;
RBF;
FGM;
Orthotropic;
T-Shape;
Triangular;
L-Shape

ABSTRACT

The torsional study of different engineering sections made up of orthotropic and functionally graded material is presented in this paper. Prandtl's stress function approach is used for the formulation of governing differential equations. Thin plate spline (TPS) radial basis function-based collocation meshfree method is utilized for discretization and solution of the governing differential equations. A classical power law is considered for the modeling of FGM material. A computer program is developed for the solution of the discretized partial differential equations. To assess the efficacy and accuracy of the present mesh-free approach, a numerical example of an equilateral triangle is considered to conduct a convergence and accuracy test. Finally, the torsional stiffness and shear stress for the orthotropic and FGM sections of the equilateral triangle, L-section, and T-sections are computed. The novelty in the present meshfree methodology lies in the handling of the singular behavior of re-entrant corners. The effect of stress concentration can be seen at the re-entrant corners. The proposed methodology shows excellent performance in solving these types of torsion problems.

1. Introduction

These engineering structures made of composites and functionally graded material (FGM) are widely used in process industries, aeronautical structures, and construction industry, and many more. FGM materials are generally inhomogeneous bodies consisting of two or more elements whose volume percentages change throughout the body. With the use of FGM in the structures, the problems associated with delamination in the layered structures are mitigated and also FGMs can be made to satisfy the specific design requirements. Beams made up of thin-walled sections such as angle, L, T, and other shapes are also subjected to a twisting moment in addition to the bending moment. The torsional rigidity of such thin-walled sections is much less in comparison to other sections. Torsional rigidity plays an important role in the proper functioning of engineering structures as it limits torsional deformations. Torsion problems become even more important in the case of the sections of low tensile strength structures. The necessity for investigating the torsional characteristics of such thin-walled noncircular cross-sections of the prismatic bar has risen significantly with the development of geometrically complicated sections composed of composites and FGM. Torsional analysis of engineering structures with non-circular cross-sections is important for the assessment of their stiffness and the stresses induced therein.

* **Corresponding author.**
E-mail address: rbpme@mmmut.ac.in

Cite this article as:

Therefore, the study of torsional problems of non-circular cross-sections is of the interest of many researchers. The classical theory for the analysis of the torsion problem is well documented in the reference books [1–4] where closed-form solutions to the torsion problem of homogeneous isotropic cross-sections such as elliptical, rectangular, and triangular sections are discussed. General theory related to the torsion problem of non-homogeneous prismatic bars and its simple solution is given by Chen [5]. Ely and Zienkiewicz [6] investigated the torsion of the nonhomogeneous and compound prismatic bar using the finite difference method. A mathematical model is derived, and solutions are presented for the strain-stress analysis of torsion of a non-circular bar [7]. An analytical solution for the torsion of the rectangular prismatic bar using a power fit model is presented by Danao and Cabrera [8]. The exact solution for the torsion of elastic circular bars of radially inhomogeneous, cylindrically orthotropic materials is presented with end effects by Tarn and Chang [9]. Rooney and Ferrari [10] presented an analytical solution for the torsion of a circular cylindrical bar with angular symmetry with inhomogeneous shear moduli. Some authors have presented an exact analytical solution for the multi-layered inhomogeneous composite bar subjected to torsion [11,12]. An exact solution in terms of the Fourier series is presented for the Saint-Venant torsion of orthotropic bars with an inhomogeneous rectangular cross-section [13]. Arghavan and Hematiyan [14] presented an analytical solution to the torsion of thin to moderately thick-walled functionally graded hollow tubes of arbitrary shapes. Ecsedi [15] presented analytical solutions of non-homogeneous cylindrical bars made up of functionally graded twisted elastic cylinders. Krahula and Lauterbach [16] used the finite element method for the torsion problem utilizing both the warping function and Prandtl's stress function approach. The finite element method has been used for the evaluation of the torsional rigidity of reinforced concrete bars with arbitrary cross-section [17] and composite beams [18]. The finite element method is used for the solution of the Saint-Venant torsion and bending problems for prismatic beams [19] and to determine the torsional stress in simply connected non-circular cross-sections [20]. Torsional analysis of bars with arbitrary cross-sections subjected to warping employing the strain-gradient elasticity has been done using the finite element method [21]. Tsiatas and Babouskos [22] presented a new integral equation solution to the elastic-plastic problem of functionally graded bars under torsional loading. A hybrid finite element approach is used for determining torsional rigidity and maximum shear stresses of arbitrarily shaped orthotropic composite or functionally graded material sections [23]. Ecsedi and Baksa [24] presented an approximate solution for the torsion and Prandtl's stress functions of an elastic cylindrical orthotropic solid elliptical cross-section. The formulation based on the boundary value problem to study the effect of material inhomogeneity on torsional response is carried out by Horgan and Chan [25]. Thereafter, Horgan [26] presented the formulation of the torsion of functionally graded anisotropic linearly elastic bars in terms of a Neumann-type boundary-value problem for the warping function. Sapountzakis [27] utilized the boundary element method to analyze the nonuniform torsion of multi-material bars. Katsikadelis and Tsiatas [28] employed the boundary element method for the torsion problem of non-homogeneous anisotropic non-circular prismatic bars. Utilizing the mesh and integral free method, Nikmehr and Lashkarbolok [29] obtained torsional rigidity of bars with functionally graded material cross-sections weakened by cracks. The torsional analysis of a bar with multiple cross-sections has been studied using the method of fundamental solution [30]. Torsion of uniform bars with polygon cross-section using Trefftz integral is presented by Hassenpflug [31].

Several analytical approaches for addressing such structural engineering issues have been developed, but these analytical methods can only be used for situations with simple geometry and loading conditions. Numerical techniques have been a valuable tool for the study of complicated engineering issues with the development of rapid computational facilities. The primary benefit of numerical techniques is that they can handle actual geometrical shapes and loadings, as opposed to the limited shapes and loadings that analytical methods can handle. Widely used numerical methods are finite difference method (FDM) and finite element methods (FEM). FEM is currently commonly utilized to solve issues with complex geometry, however, discretizing the domain with complex geometry is costly and time-consuming. In the recent past, more general methods known as meshless methods are in use that avoid the problem of mesh generation. This meshless method allows a numerical simulation process to be built solely from a collection of nodes, without the need for any pre-specified connection between them.

The radial basis function [32] is employed as a solution methodology for the analysis of prismatic bars. Chen et al [33] used the finite volume method for the torsion of homogeneous and composite bars. Ferreira [34] employed a poly-harmonic thin plate RBF for the bending

response of layer-wise modeled laminated and sandwich plates. Different types of meshfree methods in detail can be found in the reference book [35]. Hardy [36] presented the multiquadric equations of the topography and other irregular surfaces. However, several researchers have also utilized the RBF-based mesh-free method for the analysis of beams and plates [37–39] and elastic-plastic torsional analysis of prismatic bars [40]. A detailed review of the mesh-free approach for the linear and nonlinear analysis of sandwich plates is presented by Solanki et al. [41]. Ferreira et al. [42–44] presented the multiquadric radial basis function method and trigonometric shear deformation theory for the bending analysis of isotropic, laminated, and sandwich plates. The radial basis function-based collocation method is used by many researchers [45–47] for solving partial differential equations. Singh and Shukla [48] presented the RBF RBF-based mesh-free method for the nonlinear flexural analysis of laminated composite plates and functionally graded plates [49]. Shukla and Singh [50] utilized the RBF RBF-based Meshfree method for the modeling and analysis of cross-ply and angle-ply laminated plates under patch loads and the buckling behavior of rectangular angle-ply laminated composite plates [51].

From the literature review, it is evident that RBF-based mesh-free methods have been used for different cases of bending, buckling, and vibrations of plates, and up to some extent for torsional analysis of non-circular bars made up of composite and FGM materials. However, relatively less attention is paid to the torsional analysis of engineering structures with a thin-walled non-circular cross-section using the mesh-free collocation method. Therefore, the present work is focused on the torsional analysis of orthotropic and FGM prismatic bars of an equilateral triangle, L-beam, and T-beam using the thin-plate spline RBF-based meshfree collocation method. The geometry of the torsional problem is selected as an equilateral triangle with no re-entrant corner, an L-section with a single re-entrant corner, and a T-beam with two re-entrant corners. The geometry of the problem is created using scattered nodes in the entire domain. Therefore, it is easy to assign any value like the variable material property, shear modulus, etc. conveniently on the desired nodes. The novelty of the present work lies in the handling of the singular behavior of re-entrant corners as the mesh-free collocation method is a truly meshless method where the mesh elements are not required to model the geometry.

2. Mathematical Formulation

Prismatic bars of engineering sections subjected to twisting moment Mt are considered for the analysis as shown in Fig.1.

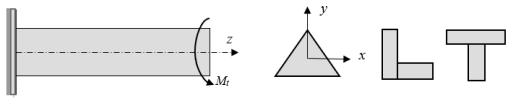

Fig.1 Prismatic bar of different cross-sections subjected to twisting moment.

The bar is fixed at z = 0 and is twisted by angle θ along the length. It is assumed that the cross-sections rotate as a rigid body. In the case of a non-circular shape, the cross-section does not remain planar and deflects in the z-direction. It is further assumed that the deflection and angle of twist θ are constant along the whole length of the bar. Thus, reducing the problem to a two-dimensional one.

According to the Saint-Venant theory, the displacements u, v, and w in directions x, y, and z respectively, can be written as:

$$u = -\theta zy, v = \theta zx, w = \theta\psi(x, y) \quad (1)$$

where ψ (x, y) is a warping function describing the deflection in the z-direction. The strain components are expressed as:

$$\varepsilon_x = \frac{\partial u}{\partial x} = 0 \; ; \; \varepsilon_y = \frac{\partial v}{\partial y} = 0 \; ; \; \varepsilon_z = \frac{\partial w}{\partial z} = 0 \quad (2)$$

$$\gamma_{xy} = \frac{\partial u}{\partial y} + \frac{\partial v}{\partial x} = 0 \quad ; \quad \gamma_{yz} = \frac{\partial v}{\partial z} + \frac{\partial w}{\partial y} = \frac{\partial w}{\partial y} + \theta x \; ;$$

$$\gamma_{xz} = \frac{\partial u}{\partial z} + \frac{\partial w}{\partial x} = \frac{\partial w}{\partial x} - \theta y \quad (3)$$

Utilizing the equation (3), the stress components are expressed as,

$$\tau_{xz} = G_{xz}\gamma_{xz} = G_{xz}\left(\frac{\partial w}{\partial x} - \theta y\right);$$

$$\tau_{yz} = G_{yz}\gamma_{yz} = G_{yz}\left(\frac{\partial w}{\partial y} + \theta x\right) \quad (4)$$

whereas other stress components are zero. Prandtl's stress function can be written as

$$\tau_{xz} = \frac{\partial \phi}{\partial y}; \tau_{yz} = -\frac{\partial \phi}{\partial x} \quad (5)$$

Therefore,

$$\tau_{xz} = G_{xz}\left(\frac{\partial w}{\partial x} - \theta y\right) = \frac{\partial \phi}{\partial y} \quad (6)$$

$$\tau_{yz} = G_{yz}\left(\frac{\partial w}{\partial y} + \theta x\right) = -\frac{\partial \phi}{\partial x} \quad (7)$$

The first two equilibrium equations are satisfied identically and the third equilibrium equation in conjunction with equations (6) and (7) yields.

$$\frac{1}{G_{yz}}\frac{\partial^2\phi}{\partial x^2}+\frac{1}{G_{xz}}\frac{\partial^2\phi}{\partial y^2}=-2\theta \qquad (8)$$

where ϕ(x,y) is Prandtl's stress function. Gxz and Gyz are the shear moduli of the material and θ is the twist angle per unit length. The equation (8) can be rewritten as,

$$\frac{\partial^2\phi}{\partial x^2}+\frac{G_{yz}}{G_{xz}}\frac{\partial^2\phi}{\partial y^2}=-2\theta G_{yz}$$

$$\text{or, } \frac{\partial^2\phi}{\partial x^2}+\alpha^2\frac{\partial^2\phi}{\partial y^2}=-2\theta G_{yz} \qquad (9)$$

where the shear modulus ratio can be defined as, . For isotropic material, Gyz= Gxz=G, the above equation (9) reduces to,

$$\frac{\partial^2\phi}{\partial x^2}+\frac{\partial^2\phi}{\partial y^2}=-2G\theta \qquad (10)$$

The boundary condition can be proved as,

$$\phi=0 \text{ on } \partial\Omega \qquad (11)$$

Resultant shear stress can be represented as,

$$\tau=\sqrt{\tau_{xz}^2+\tau_{yz}^2} \qquad (12)$$

3. Solution Methodology

The cross-sections of the equilateral triangle, L-section, and T-section are shown in Fig. 2. The dimension of the equilateral triangle is taken as 3 units on each side. The dimensions of the L-section are 3x3 (Base =3 units, Height =3 units) with web and flange thickness are 1 unit each. The geometry of these sections along with internal nodes and external nodes on the boundary are generated using computer programming.

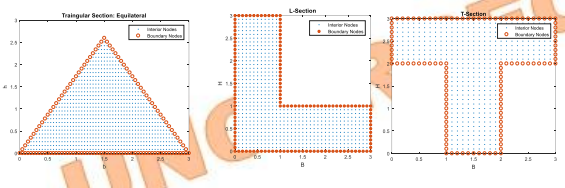

Fig.2 Equilateral Triangle, L-section, and T-section with internal and external nodes

The governing differential equation (9) and boundary condition (11) are discretized using the radial basis function. Radial basis function-based meshless formulation works on the principle of interpolation of scattered data over the entire domain.

The variable ϕ can be interpolated in the form of the radial distance between nodes. The solution of the governing differential equations is assumed in thin-plate spline (TPS) radial basis function for nodes 1: N, as,

$$\phi=\sum_{j=1}^{N}(\alpha_j^{\phi})\; g\left(\left\|X-X_j\right\|,\mathrm{c}\right) \qquad (13)$$

where $g=r^{2c}\log(r)$ with the optimized value of shape parameter c=3 for the present problem and the radial distance between two points.
where, N is the total number of nodes, which are equal to the summation of boundary nodes NB and domain interior nodes NI α_j^{ϕ}. are unknown coefficients to be evaluated.

The left-hand side of Eqn. (9) can be discretized as,

$$\left[K_I\right]_{NI\times N}=\sum_{i=1}^{NI}\sum_{j=1}^{N}\left\{\alpha_j^{\phi}\right\}\left[\frac{\partial^2 g_{(i,j)}}{\partial x^2}+\alpha^2\frac{\partial^2 g_{(i,j)}}{\partial y^2}\right] \qquad (14)$$

Similarly, boundary condition (11) can be discretized as,

$$\left[K_B\right]_{NB\times N}=\sum_{i=NI+1}^{N}\sum_{j=1}^{N}\left\{\alpha_j^{\phi}\right\}\left[g_{(i,j)}\right] \qquad (15)$$

The above problem in matrix form is expressed as,

$$\begin{bmatrix}[K]_I\\ [K]_B\end{bmatrix}_{N\times N}\left\{\alpha_j^{\phi}\right\}_{N\times 1}=\begin{Bmatrix}-2*G_{yz}*\theta\\ 0\end{Bmatrix}_{N\times 1} \qquad (16)$$

The unknown coefficients are calculated from equation (16) and finally using equation (13), the Prandtl's stress function ϕ at desired locations is obtained as,

$$\{\phi\}_{N\times 1}=\left[g\left(\left\|X-X_j\right\|,\mathrm{c}\right)\right]_{N\times N}\left\{\alpha_j^{\phi}\right\}_{N\times 1} \qquad (17)$$

The shear stresses are calculated as,

$$\left\{\tau_{xz}\right\}_{N\times 1}=\left[\frac{\partial g_{(i,j)}}{\partial y}\right]_{N\times N}\left\{\alpha_j^{\phi}\right\}_{N\times 1} \qquad (18)$$

$$\left\{\tau_{yz}\right\}_{N\times 1}=\left[-\frac{\partial g_{(i,j)}}{\partial x}\right]_{N\times N}\left\{\alpha_j^{\phi}\right\}_{N\times 1} \qquad (19)$$

Once the Prandtl's stress function ϕ is obtained, the twisting moment can be

determined using the following expression: Twisting Moment $M_t = GJ\theta = 2\iint_\Omega \phi dxdy$ (20)

The torsional stiffness and maximum shear stress for isotropic equilateral triangle beam are determined using the following expressions:

Dimensionless Torsional Stiffness,

$$\beta = \frac{J}{A^2} \quad (21)$$

Dimensionless Maximum Shear Stress,

$$\bar{\tau}_{\max} = \frac{\tau_{\max}}{\sqrt{A}G\theta} \quad (22)$$

where A is the area of the equilateral triangle. For an orthotropic equilateral triangle,

Dimensionless Torsional Stiffness,

$$\beta = \frac{GJ}{A^2 G_{xz}} \quad (23)$$

Dimensionless Maximum Shear Stress,

$$\bar{\tau}_{\max} = \frac{\tau_{\max}}{\sqrt{A}G_{xz}\theta} \quad (24)$$

4. Results and Discussion

4.1 Convergence and Accuracy Test

The convergence and accuracy tests are performed for the equilateral triangle, L-beam, and T-beam to select the number of nodes till little or no significant difference is observed in the results. The results obtained for dimensionless torsional stiffness and dimensionless maximum shear stress for equilateral triangle beam are shown in Table 1. The value of the shear modulus of rigidity and angle of twist is assumed as unity. Fig. 3 shows the convergence test for the equilateral triangle for the maximum shear stress. It can be observed that very good convergence is obtained at the nodes of 961 and beyond for torsional stiffness and maximum shear stress. In the present analysis, 961 nodes are taken in order to have better accuracy in the results. As can be seen, the present results are in close agreement with the theoretical result, therefore it shows showing efficacy and accuracy of the present solution methodology. It can be seen from Fig.4 that at 1729 nodes and beyond the percentage difference in the results are within 0.1%. Therefore, the number of nodes for all the further analysis is taken as 1729.

The torsional stiffness and maximum shear stress for the T section are computed and tabulated in Table 3. The convergence test results are depicted in Fig. 5.

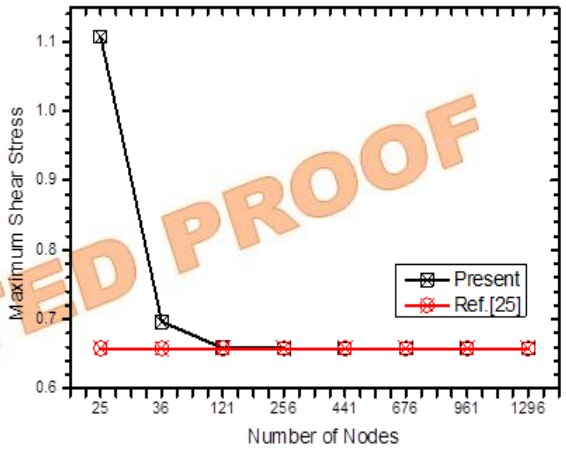

Fig. 3 Convergence test for the equilateral triangle

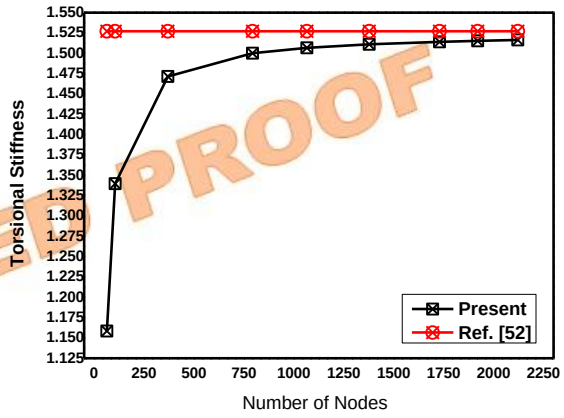

Fig. 4 Convergence test for L-section beam

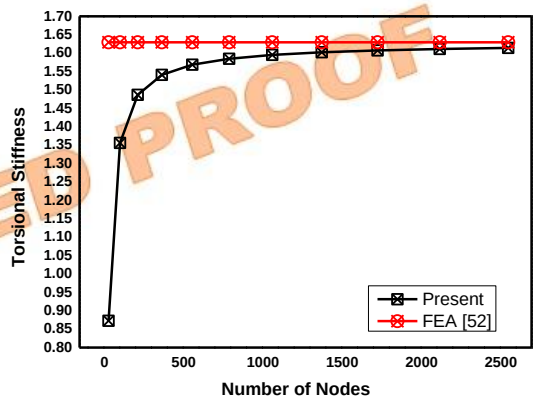

Fig. 5 Convergence test for T-section

Table 1: Convergence and validation study for the equilateral triangle

No. of Nodes	(β)	Error %	Max. Shear Stress ($\bar{\tau}_{max}$)	Error %
25	0.1005	-12.99	1.1070	68.24
36	0.1123	-2.77	0.6964	5.84
121	0.1182	2.34	0.6588	0.12
256	0.1185	2.60	0.6583	0.05
441	0.1182	2.34	0.6582	0.03
676	0.1179	2.08	0.6581	0.02
961	0.1176	1.82	0.6581	0.02
1296	0.1174	1.65	0.6581	0.02
Ref. [31]	**0.1155**		**0.6580**	

Table 2: Convergence study for L section

No. of Nodes	Torsional Stiffness (GJ)	Error %	Max. Shear Stress (τmax)	Error %
64	1.1585	24.14	0.7702	55.70
105	1.3397	12.27	1.0720	38.34
369	1.4716	3.63	1.2013	30.90
793	1.5002	1.76	1.4603	16.00
1065	1.5067	1.34	1.5612	10.20
1377	1.5110	1.05	1.6504	5.07
1729	1.5141	0.85	1.7307	0.45
1920	1.5153	0.77	1.7682	1.71
2121	1.5164	0.70	1.8041	3.77
FEA[52]	**1.5271**		**1.7385**	

Table 3: Convergence study for T-section

No. of Nodes	Torsional Stiffness (GJ)	Error %	Max. Shear Stress (τmax)	Error %
33	0.8727	46.44	1.3815	27.36
105	1.3560	16.77	1.1511	39.47
217	1.4865	8.76	1.1227	40.97
369	1.5408	5.43	1.2999	31.65
561	1.5686	3.73	1.4505	23.73
793	1.5848	2.73	1.5745	17.21
1065	1.5951	2.10	1.6810	11.61
1377	1.6023	1.66	1.7751	6.66
1729	1.6074	1.34	1.8598	2.21
2121	1.6113	1.10	1.9371	1.86
2553	1.6142	0.93	2.0086	5.62
3025	1.6166	0.78	2.0751	9.11
FEA[52]	1.6293		1.9018	

It can be seen from Fig.5 that the percentage difference in the results is within 0.1% at the nodes of 2121 and beyond. Therefore, the number of nodes for all the further analysis of the T-beam is taken as 2121. It is seen from the above convergence and validation study that the proposed mesh-free method gives very good agreement with the reference results obtained by finite element analysis (FEA). New results are reported in the next section by varying the material properties.

4.2 Orthotropic Beams

The torsional property of the beam can be altered by using orthotropic material as per desired need. In this section, the torsional analysis of the orthotropic beam is considered by varying the shear modulus ratio (Gyz/Gxz). The dimensionless torsional stiffness (β) and dimensionless maximum shear stress ($\overline{\tau}_{max}$) for equilateral triangles are calculated and tabulated in Table 4.

Table 4: Effect of Gyz/Gxz ratio on dimensionless torsional stiffness and dimensionless max shear stress for the equilateral triangle

Gyz/Gxz	β	$\overline{\tau}_{max}$
1	0.1176	0.6581
2	0.1604	0.9673
3	0.1852	1.1663
5	0.2139	1.4202
10	0.2453	1.7410
20	0.2671	2.0214
30	0.2760	2.2196
40	0.2808	2.3534
50	0.2839	2.4414

As the shear modulus ratio increases the value of the torsional stiffness and maximum shear stress increases. The higher value of the shear modulus ratio can be taken for increased torsional stiffness while designing a beam of the equilateral triangular cross-section.

The contours of Prandtl stress function and shear stresses are obtained and shown in Fig. 6. It shows the variation of Prandtl's stress function and shear stresses over the entire domain. The contours are plotted by varying the orthotropy ratio (Gyz/Gxz). It can be observed that the value of resultant shear stress at the corner of the equilateral triangle is zero and maximum at the middle of sides as expected. The computed Prandtl's stress function at the center is maximum and zero on the boundary of the triangular section. The variation in the shear stresses τxz and τyz can be observed along the bottom surface of the triangle and along the left or right surface of the triangle, respectively.

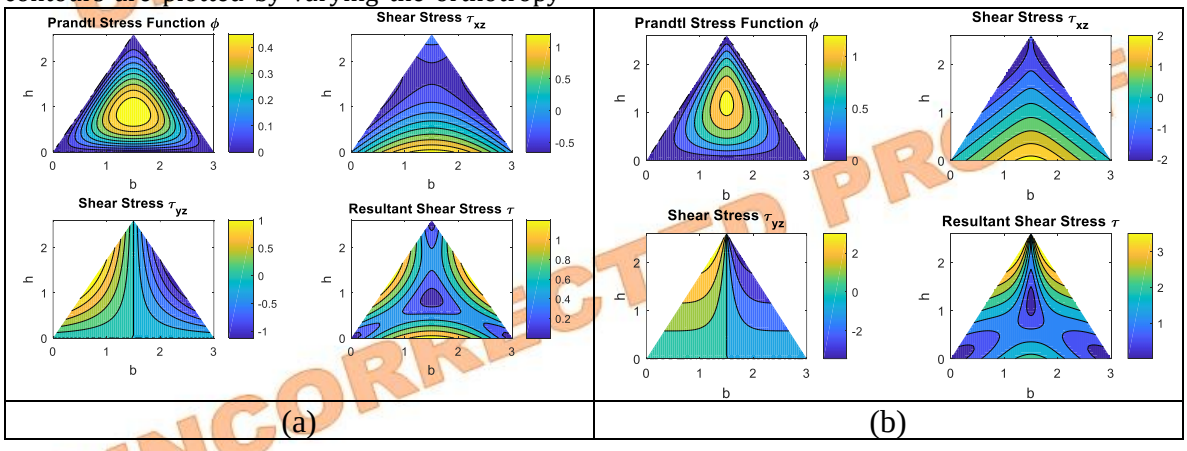

Fig.6 The contours of Prandtl's stress function and shear stress for the orthotropic equilateral triangle at (a) Gyz/Gxz = 1 and (b) Gyz/Gxz = 20

Now the effect of the orthotropy ratio on the torsional stiffness and maximum shear stress is computed for the L-beam and shown in Table 5. It can be seen that the torsional stiffness and maximum shear stress increase with the increase in the orthotropy ratio.

Figure 7 shows the contours of Prandtl stress function (ϕ), shear stress in the x-direction (τxz),

shear stress in the y-direction (τyz) and resultant shear stress (τ) for L-beam. It shows the variation of Prandtl's stress function and shear stresses over the entire domain. It can be seen that the obtained Prandtl's stress function at the center of the L-section junction is maximum. The resultant shear stress vanishes at the external corners of the L-beam and is maximum due to stress concentrations at the junction (re-entrant corner) of the flange and web of the L-beam. The variation in the shear stresses τxz and τyz can be observed along the bottom side of the L-section and along the left or right side of the L-section, respectively.

Figure 8 shows the contours of Prandtl stress function (ϕ), shear stress in the x-direction (τxz), shear stress in the y-direction (τyz) in two dimensions, and resultant shear stress (τ) in isometric view for the T-beam. It shows the variation of Prandtl's stress function and shear stresses over the entire domain. It can be seen that the obtained Prandtl's stress function is maximum near the center of the T-section junction. The

resultant shear stress vanishes at the external corners of the T-beam. The resultant shear stress is maximum at both junctions (re-entrant corners) of the web and flange of the T- T-T-section due to stress concentrations.

Table 5: Effect of Gyz/Gxz ratio on torsional stiffness and max shear stress for L-Section

Gyz/Gxz	GJ	τmax
1	1.5141	1.7307
2	2.1662	2.7671
3	2.6838	3.6029
5	3.4817	4.9125
10	4.7351	7.0780
20	5.9696	9.7584
30	6.5975	12.0893
40	6.9864	13.9932
50	7.2552	15.6385

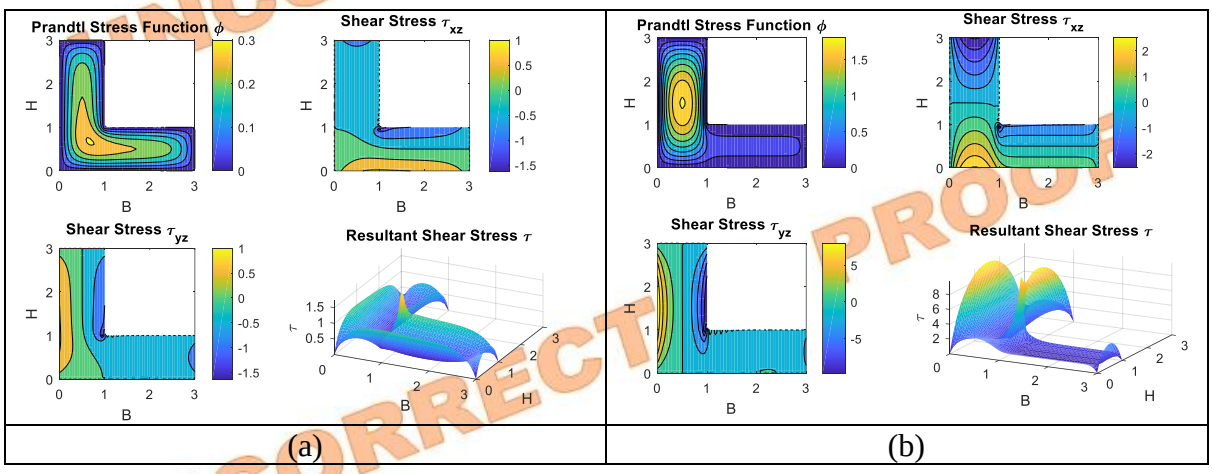

Fig.7 The contours of Prandtl's stress function and shear stress for orthotropic L-section at (a) Gyz/Gxz = 1 and (b) Gyz/Gxz = 20

To study the effect of the orthotropy ratio, the torsional stiffness and maximum shear stress are computed for the T-beam and shown in Table 6. There are two re-entrant corners in the T-beam.

Cross-section, formed at the junction of the web and flange. It can be seen that the torsional stiffness and maximum shear stress increase with the increase in the orthotropy ratio.

Table 6: Effect of Gyz/Gxz ratio on torsional stiffness and max shear stress on T-Section

Gyz/Gxz	GJ	τmax
1	1.6113	1.9371
2	2.2831	2.9872
3	2.8053	3.8284
5	3.6004	5.1510
10	4.8365	7.3571
20	6.0462	9.8919
30	6.6600	12.0466
40	7.0401	13.8464
50	7.3028	15.3813

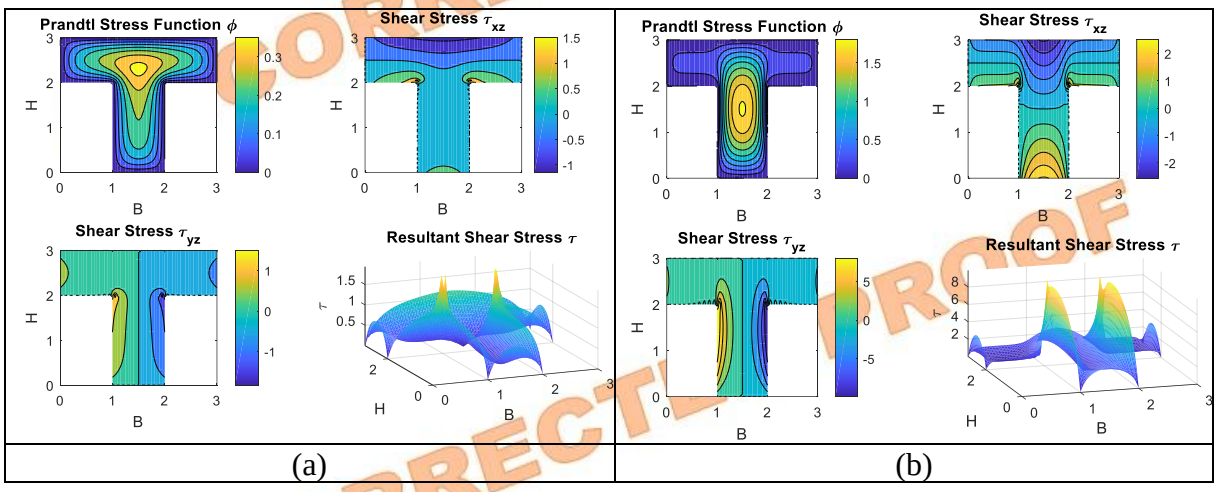

Fig. 8 The contours of Prandtl's stress function and shear stress for orthotropic L-section at (a) Gyz/Gxz = 1 and (b) Gyz/Gxz = 20

It can be concluded that the proposed meshfree method is capable of modeling the singular behavior of the re-entrant corners as evident from the L-section and T-section analysis presented in this section. A similar study for the simulation of re-entrant corners is presented [33] in which it is shown that the finite volume method (FVM) is better than the finite difference method (FDM) approach for the modeling of re-entrant corners. However, the present meshfree method can be used in a simple form to model the re-entrant corners.

4.3 Functionally Graded Material (FGM) beams

FGM materials are widely used for structural engineering purposes. The torsional behavior of the beam can be changed by employing the FGM section for a specific application. In this section, the torsional analysis of the FGM beam is considered by varying the shear modulus from the bottom to the top of the section. The distribution of shear modulus is considered to vary from bottom to top along the y-axis of the rectangular FGM section according to a classical power law. Fig. 9. shows the distribution of the shear modulus of the FGM section.

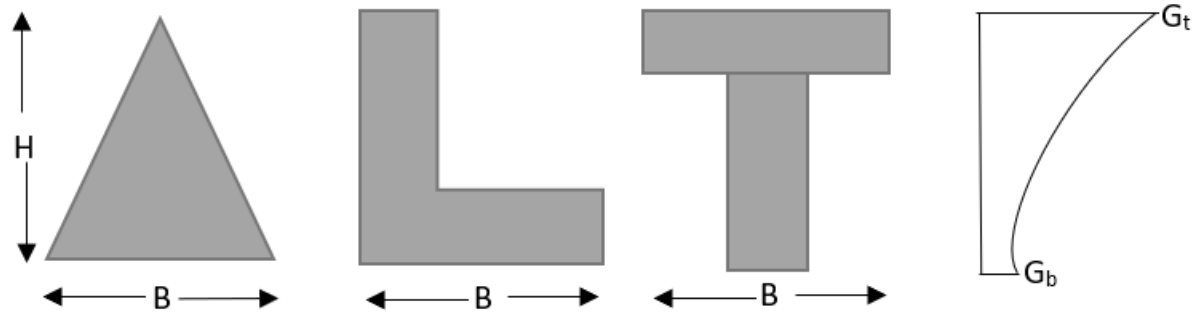

Fig.9. Distribution of the shear modulus of FGM section

The equation for the distribution of shear modulus is given by classical power law,

$$G(y) = G_b + (G_t - G_b).(y/H)^{\lambda} \qquad (25)$$

in which Gb and Gt are the shear moduli at the bottom (y=0) and top (y=h) respectively. λ is the gradient factor. When (λ=0), the material becomes homogeneous. The dimensionless torsional rigidity and dimensionless maximum shear stress for an equilateral triangle is given by,

Dimensionless Torsional rigidity,

$$\beta = \frac{GJ}{A^2 G_b} \qquad (26)$$

Shear stress factor,

$$\bar{\tau}_{\max} = \frac{\tau_{\max}}{\sqrt{A} G_b \theta} \qquad (27)$$

The dimensionless torsional stiffness (β) and dimensionless maximum shear stress ($\bar{\tau}_{\max}$) for equilateral **triangles** are calculated and tabulated in **Table 7** and **Table 8** respectively.

Table-7. Effect of different and λ on torsional stiffness of equilateral triangle

Torsional Stiffness (β)							
G. F. (λ) / G_t / G_b	0	0.5	1	3	5	7	10
1	0.1176	0.1176	0.1176	0.1176	0.1176	0.1176	0.1176
5	0.5880	0.3045	0.1982	0.1222	0.1180	0.1176	0.1176
10	1.1760	0.5381	0.2989	0.1279	0.1185	0.1177	0.1176
20	2.3519	1.0053	0.5005	0.1393	0.1195	0.1178	0.1176
40	4.7038	1.9398	0.9035	0.1622	0.1216	0.1180	0.1176

The effect of the gradient index on the dimensionless torsional stiffness is plotted in Fig. 10 with various shear modulus ratios varying from the bottom to the top of the equilateral triangle. It can be seen from Fig.10 that as the shear modulus ratio increases the torsional stiffness of the equilateral triangle increases and with the increase in the gradient index the torsional stiffness decreases. It can further be observed that the effect of the gradient index is negligible beyond 3 for the equilateral triangle considered here.

Table-8. Effect of different and λ on maximum shear stress of equilateral triangle

Max. Shear Stress ($\bar{\tau}_{max}$)							
G. F. (λ) / G_t / G_b	0	0.5	1	3	5	7	10
1	0.6581	0.6581	0.6581	0.6581	0.6581	0.6581	0.6581
5	3.2904	1.8703	1.2506	0.6914	0.6603	0.6582	0.6581
10	6.5808	3.4003	2.0328	0.7402	0.6630	0.6585	0.6581
20	13.1616	6.4751	3.6130	0.8647	0.6685	0.6589	0.6581
40	26.3232	12.6261	6.8004	1.1895	0.6822	0.6599	0.6581

The effect of gradient index on the dimensionless maximum shear stress is depicted in Fig. 11 with various shear modulus ratios varying from bottom to top of the equilateral triangle. It can be observed that the maximum shear stress increases with the increase in the shear modulus ratio from bottom to top. However, the maximum shear stress decreases with the increase in gradient index. The contour of the Prandtl stress function, shear stress in the x-direction, shear stress in the y-direction, and resultant shear stress are shown in Fig.12 for the equilateral triangle.

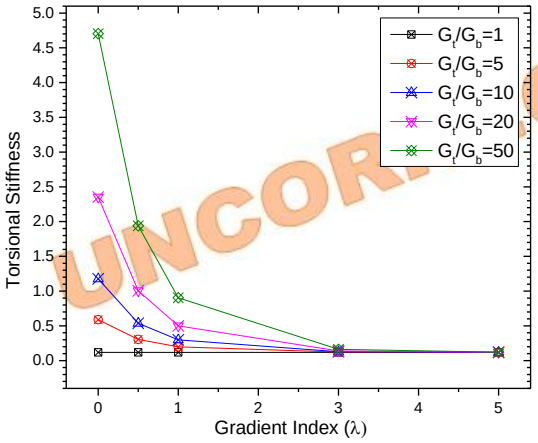

Fig. 10. Variation of torsional stiffness of equilateral triangle at different and λ

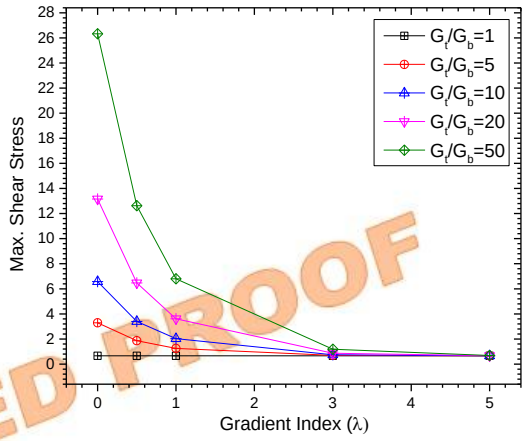

Fig. 11. Variation of maximum shear stress of equilateral triangle at different and λ

It can be observed from Fig. 12 that the Prandtl stress function is maximum near the center of the equilateral triangle and the resultant shear at the external corners is vanishing towards zero, as expected.
Now, the torsional stiffness (β) and maximum shear stress (τmax) for the L-beam are computed and tabulated in Table 9 and Table 10 respectively.

The effect of the gradient index on the torsional stiffness is plotted in Fig. 13 with various shear modulus ratios varying from the bottom to the top of the L-section.

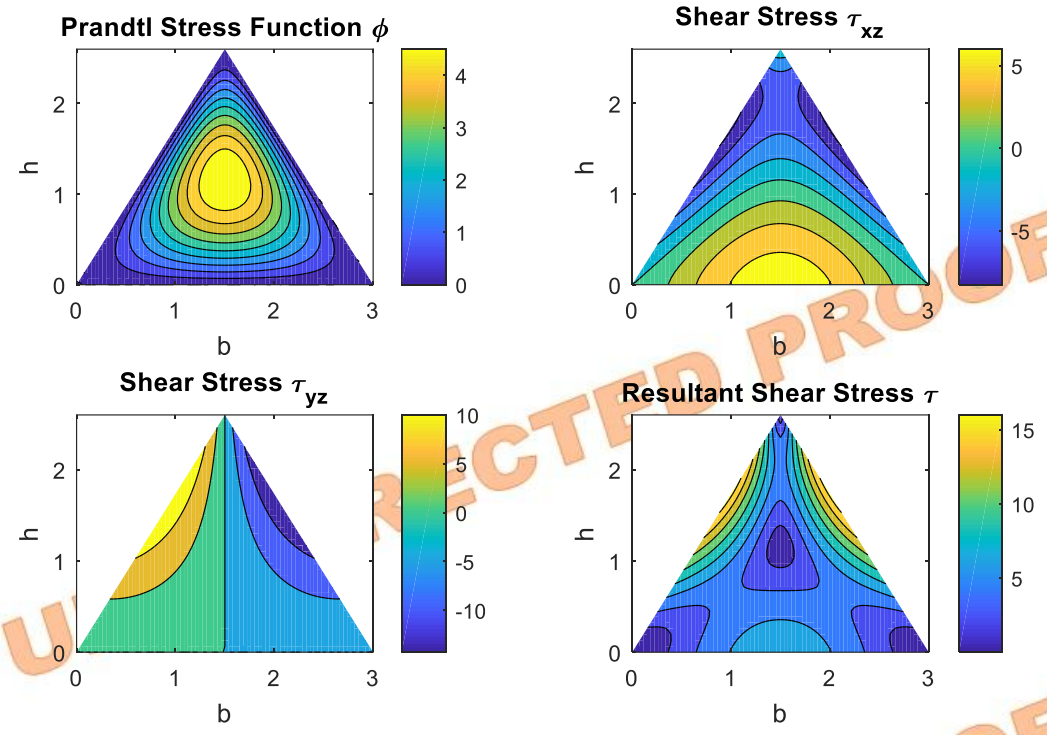

Fig. 12. Contours of Prandtl stress function and shear stress for the equilateral triangle at λ=1, Gb=1, Gt=50

Table-9. Effect of different and λ on torsional stiffness of L-shape

Torsional Stiffness (β)							
G. F. (λ) G_t / G_b	0	0.5	1	5	10	20	50
1	1.5141	1.5141	1.5141	1.5141	1.5141	1.5141	1.5141
5	7.5706	4.8398	3.6042	1.9138	1.6779	1.5718	1.5258
10	15.1411	8.9969	6.2168	2.4134	1.8825	1.6440	1.5404
20	30.2822	17.3112	11.4421	3.4126	2.2919	1.7882	1.5697
40	60.5645	33.9397	21.8926	5.4111	3.1107	2.0768	1.5981

It can be seen from Fig.13 that as the shear modulus ratio increases the torsional stiffness of the L-section increases and with the increase in the gradient index the torsional stiffness decreases. Insignificant variation in the torsional stiffness is observed beyond the gradient index of 20 for the L-beam considered here. The effect of gradient index on the maximum shear stress is depicted in Fig. 14 with various shear modulus ratios varying from bottom to top of the L-section. It can be observed that the maximum shear stress increases with the increase in the shear modulus ratio from bottom to top. However, the maximum shear stress decreases with the increase in the gradient index of the L-beam. The contour of the Prandtl stress function, shear stress in the x-direction, shear stress in the y-direction, and resultant shear stress are shown in Fig.15 for the L-beam. The effect of stress concentration at the re-entrant corners can be observed in Fig.15. This shows the utility of the present mesh-free method for the modeling of singular locations. The torsional stiffness (β) and maximum shear stress (τmax) for the T-beam are computed and tabulated in Table 11 and Table 12, respectively.

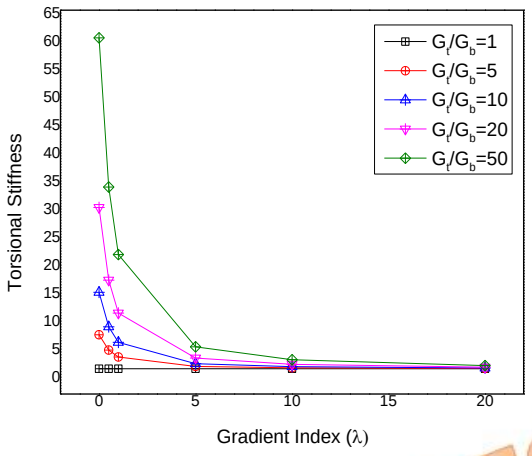

Fig. 13. Variation of torsional stiffness of L-shape at different and λ

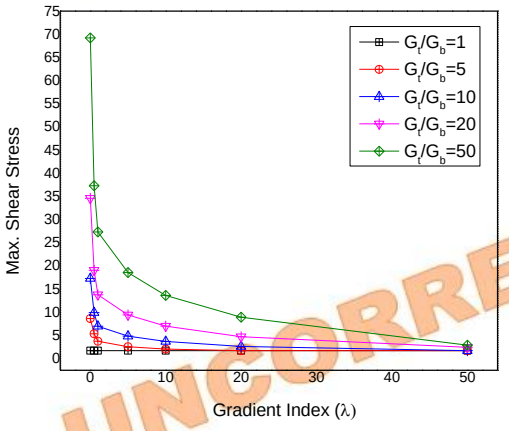

Fig. 14. Variation of maximum shear stress of L-shape at different and λ

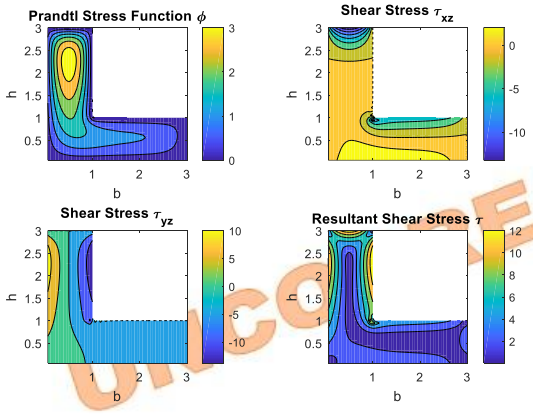

Fig. 15. Contours of Prandtl stress function and shear stress for L-beam at λ=1, Gb=1, Gt=20

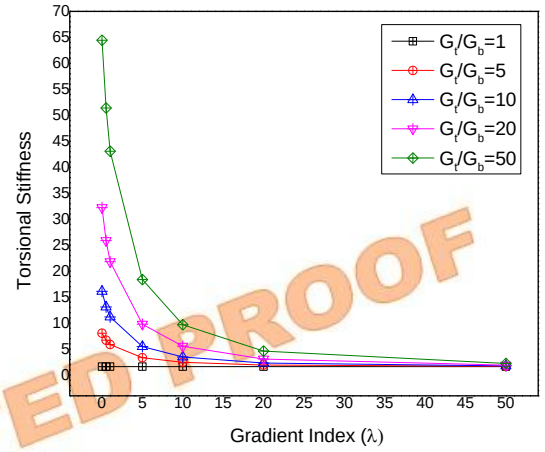

Fig. 16. Variation of torsional stiffness of T-shape at different and λ

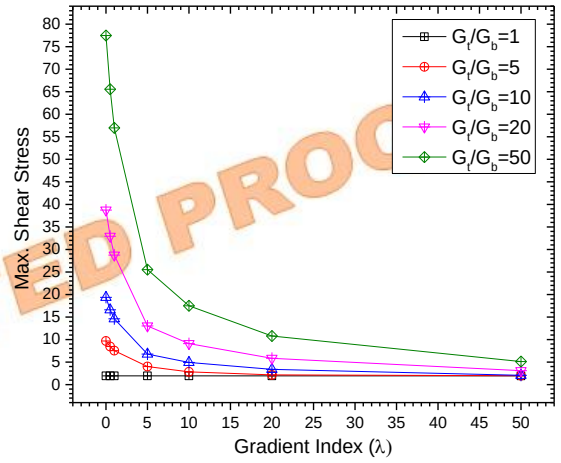

Fig. 17. Variation of maximum shear stress of T-shape at different and λ

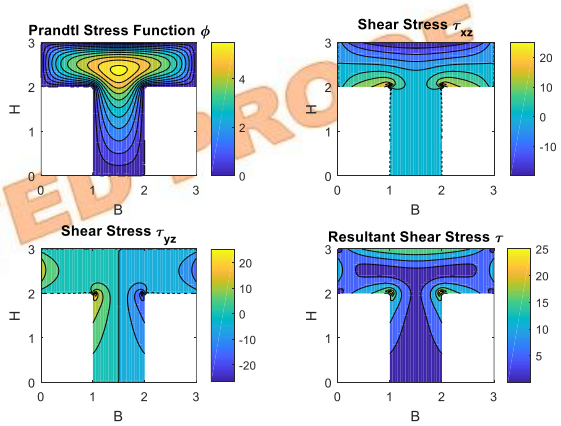

Fig. 18. Contours of Prandtl stress function and shear stresses for T-beam at λ=1, Gb=1, Gt=20

Table-10. Effect of different and λ on maximum shear stress of L-shape

Max. Shear Stress (τmax)							
G. F. (λ) G_t / G_b	0	0.5	1	5	10	20	50
1	1.7307	1.7307	1.7307	1.7307	1.7307	1.7307	1.7307
5	8.6536	5.3800	3.7585	2.5706	2.0664	1.7325	1.7310
10	17.3073	9.9427	7.0068	4.8572	3.7226	2.6376	1.7313
20	34.6145	19.0684	13.7900	9.4304	7.0350	4.7445	2.4596
40	69.2291	37.3200	27.3562	18.5767	13.6599	8.9583	2.9273

Table-11. Effect of different and λ on torsional stiffness of T-shape

Torsional Stiffness (β)							
G. F. (λ) G_t / G_b	0	0.5	1	5	10	20	50
1	1.6113	1.6113	1.6113	1.6113	1.6113	1.6113	1.6113
5	8.0563	6.7190	5.8650	3.3308	2.4391	1.9190	1.6737
10	16.1126	13.1037	11.1823	5.4802	3.4738	2.3038	1.7516
20	32.2253	25.8730	21.8167	9.7789	5.5434	3.0732	1.9076
40	64.4505	51.4117	43.0857	18.3765	9.6824	4.6121	2.2196

Table-12. Effect of different and λ on maximum shear stress of T-shape

Max. Shear Stress (τmax)							
G. F. (λ) G_t / G_b	0	0.5	1	5	10	20	50
1	1.9371	1.9371	1.9371	1.9371	1.9371	1.9371	1.9371
5	9.6857	8.4537	7.5495	4.0101	2.8222	2.1479	1.9721
10	19.3713	16.5996	14.6121	6.7723	4.9176	3.3682	2.0633
20	38.7427	32.9147	28.7372	13.0239	9.1085	5.8374	3.0827
40	77.4853	65.5621	56.9876	25.5272	17.4903	10.7759	5.1215

The effect of the gradient index on the torsional stiffness is plotted in Fig. 16 with various shear modulus ratios varying from the bottom to the top of the T-section. It can be seen from Fig.16 that as the shear modulus ratio increases the torsional stiffness of the T-section increases however, with the increase in the gradient index the torsional stiffness decreases. There is negligible change in the torsional stiffness beyond the gradient index of 50 for the T-beam considered here.

The effect of gradient index on the maximum shear stress is depicted in Fig. 17 with various shear modulus ratios varying from bottom to top of the T-section. It can be observed that the maximum shear stress increases with the increase in the shear modulus ratio from bottom to top. However, the maximum shear stress decreases with the increase in gradient index for the T-beam. The contour of the Prandtl stress function, shear stress in the x-direction, shear stress in the y-direction, and resultant shear stress are shown in Fig.18 for the T-beam.

The effect of stress concentration at the intersection of the flange and web can be observed in Fig.18. The singular location present in the T-beam is modeled effectively using the proposed mesh-free method.

5. Conclusions

The main objective of the present paper was to show the capability of the meshfree collocation method for the torsional analysis of the prismatic bars made up of non-circular cross-sections such as equilateral triangles, L-section, and T-section containing re-entrant corners. The proposed methodology is employed for the determination of torsional stiffness and shear stresses by varying the orthotropy ratio and gradient index of orthotropic and FGM sections, respectively. The results for the prismatic bar with the equilateral triangle section are compared with the numerical results published in the literature to examine the validity of the proposed method. It is found that the results are in good agreement with the published literature.

The proposed solution methodology method is presented for the triangular section with no re-entrant corner, the L-section with a single re-entrant corner, and T- the section with two re-entrant corners. The singular location at the re-entrant corners is very well handled by the proposed mesh-free methodology. The results were found to be stable and capable of modeling the singular points using thin-plate spline RBF for the problems related to the structural engineering application. The study conducted for the orthotropic sections reveals that the torsional rigidity and shear stresses increase with the increase in the orthotropy ratio. However, in the case of FGM sections, the torsional rigidity and shear stress increase with the increased shear modulus from the bottom surface to the top surface and decrease as the gradient index increases. The proposed methodology is found to be a suitable computational tool for the torsional analysis of orthotropic and FGM sections of non-circular cross-sections including the sections containing re-entrant corners. Therefore, the present mesh-free method can be extended as a computational tool for the parametric analysis of structural engineering design and for solving the torsion problem with composite and heterogenous material as well as for the curved geometry of the arbitrary shapes. Also, reinforcement of re-entrant corners can be considered for reducing the stress concentration at the re-entrant corners.

References

[1] Timoshenko S, Goodier JN. Theory of Elasticity. 3rd ed. McGraw-Hill Book Company; 1970.

[2] Muskhelishvili NI. Some basic problems of the mathematical theory of Elasticity. 2nd ed. Springer-Science+ Business Media, B.V.; 1977.

[3] Boresi AP, Schmidt RJ. Advanced Mechanics of Materials. 6th ed. John Wiley & Sons, Inc.; 2003.

[4] Sadd MH. Elasticity. 3rd ed. Elsevier Academic Press; 2014.

[5] Chen Y., 1964. Torsion of nonhomogeneous bars. *J Franklin Inst*, 277, pp 50–4.

[6] Ely JF, Zienkiewicz OC, 1960. Torsion of Compound Bars- A Relaxation Solution. *Int J Mech Sci*,1, pp 356–365.

[7] Franců J, Nováčková P, Janíček P, 2012. Torsion of a Non-Circular Bar. Eng Mech;19, pp 45–60.

[8] Angelo Danao LM, Cabrera RM. Torsion of a rectangular prismatic bar: Solution using a power fit model. Philipp Eng J 2007;28, pp 77–98.

[9] Tarn JQ, Chang HH., 2008. Torsion of cylindrically orthotropic elastic circular bars with radial inhomogeneity: some exact solutions and end effects. Int J Solids Struct ,45, pp 303–19.

[10] Rooney FJ, Ferrari M. 1995. Torsion and flexure of inhomogeneous elements. Compos Eng, 5, pp 901–11.

[11] Swanson SR. 1998 Torsion of laminated rectangular rods. Compos Struct, 42, pp 23–31.

[12] Savoia M, Tullini N., 1993.Torsional response of inhomogeneous and multilayered composite beams. Compos Struct ,25, pp 587–94.

[13] Rongqiao X, Jiansheng H, Weiqiu C. 2010, Saint-Venant torsion of orthotropic bars with inhomogeneous rectangular cross section. Compos Struct ,92, pp1449–57.

[14] Arghavan S, Hematiyan MR., 2009. Torsion of functionally graded hollow tubes. Eur J Mech A/Solids ,28, pp 551–9.

[15] Ecsedi I., 2009. Some analytical solutions for Saint-Venant torsion of non-homogeneous cylindrical bars. Eur J Mech A/Solids,28, pp 985–990.

[16] Krahula J.L., Lauterbach G.F., 1969. Finite Element Solution for Saint-Venant Torsion. AIAA J ,7, pp 2200–3.

[17] Li Z, Ko JM, Ni YQ., 2000. Torsional rigidity of reinforced concrete bars with arbitrary sectional shape. Finite Elem Anal Des,35, pp 349–61.

[18] Saygun A, Omurtag MH, Orakdogen E, Girgin K, Kucukarslan S, Darilmaz K., 2007. A simplified solution of the torsional rigidity of the composite beams by using FEM. Adv Struct Eng,10, pp 467–73.

[19] Jog CS, Mokashi IS., 2014. A finite element method for the Saint-Venant torsion and bending problems for prismatic beams. Comput Struct,135, pp 62–72.

[20] Abdelkader K, Toufik Z, Mohamed BJ., 2015. Torsional stress in non-circular cross sections by the finite element method. Adv Mech Eng,7, pp 1–20.

[21] Beheshti A., 2018. A numerical analysis of Saint-Venant torsion in strain-gradient bars. Eur J Mech A/Solids,70, pp 181–90.

[22] Tsiatas GC, Babouskos NG., 2017. Elastic-plastic analysis of functionally graded bars under torsional loading. Compos Struct ,176, pp 254–67.

[23] Darılmaz K, Orakdö E., 2018. Saint-Venant torsion of arbitrarily shaped orthotropic composite or FGM sections by a hybrid finite element 1398, pp 1387–98.

[24] Ecsedi I, Baksa A., 2019. Saint-Venant torsion of cylindrical orthotropic elliptical cross section. Mech Res Commun,99, pp 42–6.

[25] Horgan CO, Chan AM., 1998. Torsion of functionally graded isotropic linearly elastic bars. J Elast, 52, pp 181–99.

[26] Horgan CO., 2007. On the torsion of functionally graded anisotropic linearly elastic bars. IMA J Appl Math (Institute Math Its Appl, 72,pp 556–562.

[27] Sapountzakis EJ., 2001. Nonuniform torsion of multi-material composite bars by the boundary element method. Comput Struct, 79, pp 2805–16.

[28] Katsikadelis JT, Tsiatas GC., 2016. Saint - Venant Torsion of Non - homogeneous Anisotropic Bars. J Appl Comput Mech,2, pp 42–53.

[29] Nikmehr O, Lashkarbolok M., 2019. A Numerical Investigation on the Torsional Rigidity of Bars with Functionally Graded Material (FGM) Cross Sections Weakened by Cracks. Iran J Sci Technol - Trans Civ Eng ,43, pp 117–123.

[30] Gorzelańczyk P., 2010. Method of fundamental solutions and random numbers for the torsion of bars with multiply connected cross sections. Comput Assist Mech Eng Sci,17, pp 99–112.

[31] Hassenpflug WC., 2003. Torsion of Uniform Bars with Polygon Cross-Section. Comput Math with Appl, 46, pp 313–92.

[32] Kołodziej JA, Gorzelańczyk P., 2012. Application of method of fundamental solutions for elasto-plastic torsion of prismatic rods. Eng Anal Bound Elem, 36, pp 81–6.

[33] Chen H, Gomez J, Pindera MJ., 2020. Saint Venant's torsion of homogeneous and composite bars by the finite volume method. Compos Struct ,242, pp 112–128.

[34] Ferreira AJM., 2004. Polyharmonic (thin-plate) splines in the analysis of composite plates. Int J Mech Sci ,46, pp 1549–69.

[35] Liu GR., 2009. Mesh Free Methods: Moving beyond the finite element method. 2nd ed. CRC Press.

[36] Hardy RL., 1971. Multiquadric Equations of Topography and Other Irregular Surfaces. J Geophys Res,76, pp 1905–1915.

[37] Bui TQ, Nguyen MN, Zhang C., 2011. An efficient meshfree method for vibration analysis of laminated composite plates. Comput Mech ,48(2), pp 175–93.

[38] Bui TQ, Nguyen MN., 2013. Meshfree Galerkin Kriging model for bending and buckling analysis of simply supported laminated composite plates. Int J Comput Methods,10,pp 1350011.

[39] Bui TQ, Khosravifard A, Zhang C, Hematiyan MR, Golub M V., 2013. Dynamic analysis of sandwich beams with functionally graded core using a truly meshfree radial point interpolation method. Eng Struct,47,pp 90–104.

[40] Mukhtar FM, Al-Gahtani HJ., 2016. Application of radial basis functions to the problem of elasto-plastic torsion of prismatic bars. Appl Math Model,40, pp 436–50.

[41] Solanki MK, Mishra SK, Singh J. 2016. Meshfree approach for linear and nonlinear analysis of sandwich plates: A critical review of twenty plate theories. Eng Anal Bound Elem ,69, pp 93–103.

[42] Liew KM, Zhao X, Ferreira AJM., 2011. A review of meshless methods for laminated and functionally graded plates and shells. Compos Struct ,93, pp 2031–41.

[43] Ferreira AJM., 2005. Free Vibration Analysis of Timoshenko Beams and Mindlin Plates By Radial Basis Functions. Int J Comput Methods ,02, pp 15–31.

[44] Ferreira AJM, Roque CMC, Jorge RMN., 2005.Analysis of composite plates by trigonometric shear deformation theory and multiquadrics. Comput Struct 83, pp 2225–37.

[45] Fasshauer GE., 1997. Solving Partial Di erential Equations by Collocation with Radial Basis Functions. Construction, 93,pp 1–8.

[46] Fasshauer GE., 1999. Solving differential equations with radial basis functions: Multilevel methods and smoothing. Adv Comput Math, 11, pp 139–59.

[47] Franke C, Schaback R., 1998. Solving partial differential equations by collocation using radial basis functions. Appl Math Comput,93, pp 73–82.

[48] Singh J, Shukla KK.,2012. Nonlinear flexural analysis of laminated composite plates using RBF based meshless method. Compos Struct ,94, pp 1714–20.

[49] Singh J, Shukla KK., 2012. Nonlinear flexural analysis of functionally graded plates under different loadings using RBF based meshless method. Eng Anal Bound Elem ,36, pp 1819–27.

[50] Shukla V, Singh J., 2020. Modeling and analysis of cross-ply and angle-ply laminated plates under patch loads using RBF based meshfree method and new HSDT. Comput Math with Appl ,79, pp 2240–57.

[51] Shukla V, Singh J., 2020. Buckling behavior of rectangular angle-ply laminated composite plates subjected to thermal and mechanical loads using the meshfree method. Int J Comput Mater Sci Eng , 09, pp 2050021.

[52] Skyciv Section Builder Software. Skyciv Platf 2021.